ENVIRONMENTAL RESEARCH
LETTERS

LETTER • OPEN ACCESS

# A humidity-based exposure index representing ozone damage effects on vegetation

ENVIRONMENTAL RESEARCH
LETTERS

LETTER

# A humidity-based exposure index representing ozone damage effects on vegetation

Cheng Gong[1,2], Xu Yue[3,*], Hong Liao[3,*] and Yimian Ma[2,4]

[1] State Key Laboratory of Atmospheric Boundary Layer Physics and Atmospheric Chemistry (LAPC), Institute of Atmospheric Physics, Chinese Academy of Sciences, Beijing 100029, People's Republic of China
[2] University of Chinese Academy of Sciences, Beijing 100049, People's Republic of China
[3] Jiangsu Key Laboratory of Atmospheric Environment Monitoring and Pollution Control, Jiangsu Collaborative Innovation Center of Atmospheric Environment and Equipment Technology, School of Environmental Science and Engineering, Nanjing University of Information Science and Technology, Nanjing 210044, People's Republic of China
[4] Climate Change Research Center, Institute of Atmospheric Physics, Chinese Academy of Sciences, Beijing 100029, People's Republic of China
[*] Authors to whom any correspondence should be addressed.

**E-mail:** yuexu@nuist.edu.cn **and** hongliao@nuist.edu.cn

**Keywords:** ozone, exposure index, dose index, $O_3$RH, AOT40, trend

Supplementary material for this article is available online

OPEN ACCESS

RECEIVED
24 January 2021

REVISED
24 February 2021

ACCEPTED FOR PUBLICATION
8 March 2021

PUBLISHED
24 March 2021



## Abstract

Surface ozone ($O_3$) is detrimental to plant health. Traditional exposure indexes, such as accumulated hourly $O_3$ concentrations over a threshold of 40 ppb (AOT40), are easy to be derived and widely used to assess $O_3$ damage effects on vegetation. However, the regulation of environmental stresses on $O_3$ stomatal uptake is ignored. In comparison, the dose-based indexes are much more reasonable but require complex parameterization that hinders further applications. Here, we propose a new humidity-based index ($O_3$RH) representing $O_3$ damage effects on vegetation, which can be simply derived using ground-level $O_3$ and relative humidity (RH). Compared with $O_3$ damages to gross primary productivity ($GPP_d$) derived from a process-based scheme over May to October in 2015–2018, the $O_3$RH index shows spatial correlations of 0.59 in China, 0.62 in U.S., and 0.58 ($P < 0.01$) in Europe, much higher than the correlations of 0.16, −0.22, and 0.24 ($P < 0.01$) for AOT40. Meanwhile, the $O_3$RH index shows temporal correlations of 0.73 in China, 0.82 in U.S, and 0.81 ($P < 0.01$) in Europe with $GPP_d$, again higher than the correlations of 0.50, 0.67, and 0.79 ($P < 0.01$) for AOT40. Analyses of $O_3$RH reveal relatively stable trend of $O_3$ vegetation damages in eastern U.S. and western Europe, despite the long-term reductions in local $O_3$ pollution levels. Our study suggests the substitution of traditional exposure-based indexes such as AOT40 with $O_3$RH for more reasonable assessments of $O_3$ ecological effects.

## 1. Introduction

Tropospheric ozone ($O_3$) is a secondary air pollutant generated by photochemical reactions of nitrogen oxide ($NO_x = NO + NO_2$) and volatile organic compounds (Atkinson 2000, Kleinman 2005, Jacob and Winner 2009). Ambient surface $O_3$ concentrations ($[O_3]$) kept increasing by 0.5%–2% $yr^{-1}$ at the middle latitudes of the Northern Hemisphere over 1970–2000 (Vingarzan 2004). Since the 1990s, $[O_3]$ decreased in rural areas in North America and Europe (on average 0.23 ppbv $yr^{-1}$) but increased in urban areas worldwide (on average 0.31 ppbv $yr^{-1}$) (Sicard 2020). $O_3$ exposure (including acute exposure with high $[O_3]$ and chronic exposure) leads to foliar injury and reductions in plant productivity (Paakkonen *et al* 1998, Lombardozzi *et al* 2012, Yue *et al* 2017, De Marco *et al* 2020), which further influence the land carbon budget as well as the climate (Tian *et al* 2011, Arnold *et al* 2018, Gong *et al* 2020).

The intensity of $O_3$ vegetation damage depends not only on $[O_3]$, but also on environmental stresses. For example, the drought conditions with low air relative humidity (RH) and low soil-water contents

lead to closure of plants stomata, further reducing stomatal $O_3$ uptake and $O_3$ injury (Khan and Soja 2003, Hayes *et al* 2012, Gao *et al* 2017). The differences in carbon dioxide concentrations, and nitrogen loads may result in different vegetation responses to $O_3$ even with the same [$O_3$] (Topa *et al* 2004, Thomas *et al* 2006, Mishra *et al* 2013). Furthermore, differences in plant function types (PFTs) as well as phenological stages also lead to different stomatal $O_3$ uptakes (Clifton *et al* 2020b) and the consequent vegetation damages (Sitch *et al* 2007, Anav *et al* 2019). As a result, environmental stresses such as air temperature and solar radiation would indirectly regulate $O_3$ vegetation damages by influencing PFT distribution and plants phenology.

To assess the $O_3$ risks to ecosystem functions, various damaging indexes have been proposed and applied. In general, these indexes can be classified into exposure-based or dose-based groups. The accumulated $O_3$ over a threshold of 40 ppb (AOT40) is a typical exposure-based index adopted by the Long-Range Transboundary Air Pollution (CLRTAP) Convention to assess the ecological impacts of $O_3$ (Fuhrer *et al* 1997, Spranger *et al* 2004). AOT40 represents the $O_3$ exposure level using a simplified formula but is insufficient to quantify $O_3$-induced vegetation damage since the influences of environmental stresses are not considered (Emberson *et al* 2000, Mills *et al* 2011a). Many studies found that the vegetation damage was more determined by '$O_3$ uptake fluxes' entering stomata rather than $O_3$ exposure (e.g. Musselman *et al* 2006, Karlsson *et al* 2007, Mills *et al* 2011a, Bueker *et al* 2015, De Marco *et al* 2020, Clifton *et al* 2020b). As a result, the dose-based index such as phytotoxic ozone dose over a threshold flux of Y nmol $m^2$ PLA $s^{-1}$ ($POD_Y$, and PLA is the projected leaf area) is proposed to represent the stomatal flux of ozone. $POD_Y$ includes the influences of environmental stresses on stomata and thus describes $O_3$ damage effects more mechanistically and precisely (Mills *et al* 2011b).

The key step of estimating $POD_Y$ is the calculation of stomatal conductance ($g_s$), which is generally obtained by two kinds of model: the Jarvis model (Jarvis 1976, Emberson *et al* 2000, Buckley and Mott 2013) or photosynthesis-stomata ($A_{net}$-$g_s$) model (e.g. Farquhar *et al* 1980, Ball *et al* 1987). The Jarvis model calculate $g_s$ by multiplying PFT-specific maximum $g_s$ (provided by published observational data) and a series of factors representing influences of environmental stresses (including temperature, vapor pressure deficit (VPD), soil water content and solar radiation) and phenology (Spranger *et al* 2004). It is effective to assess $O_3$ vegetation damages at single-site level (e.g. Bueker *et al* 2012, 2015), but the complexity in calculating each factor and the difficulties in obtaining observed input data (such as photosynthetic photon flux density, soil water potential, quasi-laminar resistance ($r_b$) and leaf surface resistance ($r_c$)) limit the application of Jarvis model when upscaling to regional or global scales. The $A_{net}$-$g_s$ model derives $g_s$ by coupling photosynthesis rates based on physiological relationships (Clifton *et al* 2020a). It has been widely applied in dynamic global vegetation models (DGVMs) or land-surface models (Yue and Unger 2015, Sadiq *et al* 2017), making the large-scale evaluation possible but requiring proficient coding skills and high computing resources.

Because of the complexity in deriving $POD_Y$, the exposure-based indexes are still widely used to assess $O_3$ ecological effects, especially in the atmospheric chemistry community (e.g. Sicard *et al* 2016, 2017, Lin *et al* 2018, Lu *et al* 2018, Mills *et al* 2018, Feng *et al* 2019), though $POD_Y$ is a better metric to assess $O_3$ ecological effects (e.g. Mills *et al* 2011a, Anav *et al* 2016, Shang *et al* 2017). Karlsson *et al* (2004) attempted to modify AOT40 as a new index named $AOT30_{VPD}$ by considering humidity impacts on $g_s$. However, the $AOT30_{VPD}$ based on subterranean clover was designed to describe the short-term visible ozone injury and thus unable to assess $O_3$ damages on ecosystem productivity (Spranger *et al* 2004). In this study, we propose a new index based on DGVMs simulations with $A_{net}$-$g_s$ model to indicate the long-term $O_3$ damage effects to ecosystem productivity. The new index named $O_3RH$ has two main advantages: (a) calculations of $O_3RH$ are as easy as AOT40 and (b) the index can represent spatiotemporal pattern of $O_3$ damage as efficient as the dose-based method. In particular, we are not denying the advances of $POD_Y$ metric, instead we propose the simplified but comparably effective $O_3RH$ index to facilitate the current assessments of $O_3$ ecological risks for atmospheric chemistry community.

## 2. Methods

### 2.1. The Yale Interactive terrestrial Biosphere (YIBs) model

The YIBs model includes nine PFTs and can dynamically simulate vegetation biophysical processes, including leaf photosynthesis ($A_{tot}$), respiration, transpiration, phenology, and carbon allocation at the global scale (Yue and Unger 2015). Stomatal conductance ($g_s$) is dependent on $A_{tot}$ following the Ball–Berry scheme (Farquhar *et al* 1980, Ball *et al* 1987):

$$g_s = m\frac{(A_{tot} - R_d) \times RH}{c_s} + b, \qquad (1)$$

where $R_d$ is the respiration rate. RH and $C_s$ indicate the RH and $CO_2$ concentration at the leaf surface, respectively. $m$ and $b$ are PFT-dependent parameters regulating stomatal conductance (see details in Yue and Unger (2015) and Gong *et al* (2020)). Previous studies have extensively validated YIBs-simulated gross primary productivity (GPP) and showed reasonable seasonality compared to site-level observations (correlation coefficients larger than 0.8) with

biases ranging from −19% to 7% depending on different PFTs (Yue and Unger 2015). In this study, we perform global simulations using the YIBs model with resolution of 1° × 1° over 2015–2018. Meteorological fields from Version 2 of Modern Era Retrospective-analysis for Research and Application (MERRA2) (Molod *et al* 2015) and observed $O_3$ (section 2.4) are used to drive the model.

### 2.2. $O_3$ damage scheme in YIBs

The $O_3$ damage ratio ($F$) to the original photosynthesis is calculated as a linear function of stomatal $O_3$ uptake fluxes ($F_{O3}$) (Sitch *et al* 2007):

$$F = a \times \max\left[F_{O_3} - F_{O_3,\mathrm{crit}}, 0.0\right], \tag{2}$$

where the PFT-specific parameters $a$ and $F_{O3,crit}$ are derived from observations (Sitch *et al* 2007, Yue and Unger 2015). The parameter $a$ has two sets of values representing varied sensitivities from low to high (see details in Sitch *et al* (2007) and Gong *et al* (2020)). $F_{O3}$ is calculated by the following formula:

$$F_{O3} = \frac{[O_3]}{R_a + \left[\frac{k_{O3}}{g_s}\right]}, \tag{3}$$

where $[O_3]$ is the ambient $O_3$ concentration and $R_a$ is the aerodynamic resistance. $k_{O3}$ is set as 1.67 to represent the ratio of leaf resistance for $O_3$ to leaf resistance for water vapor. The stomatal conductance $g_s$ is derived from equation (1). Evaluations showed that this scheme was able to simulate reasonable GPP-$O_3$ and $g_s$-$O_3$ relationships for various PFTs (Yue *et al* 2016, Yue and Unger 2018).

### 2.3. Definition of $O_3$ damaging indexes

Three widely used indexes, including maximum daily 8 h (MDA8) $[O_3]$, AOT40, and $POD_1$, are compared for $O_3$ vegetation damage:

$$\mathrm{AOT40}_d = \sum_{h=8}^{20} \max\left([O_3]_{d,h} - 40, 0\right) \tag{4}$$

$$(\mathrm{POD}_1)_d = \sum_{h=1}^{24} \max\left((F_{O_3})_{d,h} - 1, 0\right) \times 3600, \tag{5}$$

where $[O_3]_{d,h}$ is the observed $O_3$ concentrations (ppbv) at $h$ hour (local time) on $d$ day, and $(F_{O3})_{d,h}$ is the simulated stomatal $O_3$ uptake fluxes (nmol $m^{-2}$ $s^{-1}$). The $O_3$ flux threshold in $POD_Y$ is selected as 1 nmol $m^{-2}$ $s^{-1}$ following the recommendation by CLRTAP (2017) since it provides the strongest relationships (maximum $R^2$) between $O_3$ flux and vegetation damages (Bueker *et al* 2015). To account for the dependence of $O_3$ damage on $[O_3]$ and $g_s$ (equation (3)), the latter of which is related to RH (equation (1)), we propose a new RH-based $O_3$ damage index $O_3$RH as follows:

$$\mathrm{O_3RH}_d = f(O_3) \times f(\mathrm{RH}), \tag{6}$$

where the $f(O_3)$ *and* $f(RH)$ are expressed following the thresholds described in section 3.3:

$$f(O_3) = \max\left(0, \mathrm{MDA8}[O_3]_d - 20\right) \tag{7}$$

$$f(\mathrm{RH}) = \max(0, \min\left(\mathrm{RH}_d - 40\%, 40\%\right)), \tag{8}$$

where $RH_d$ is the daily-mean RH (%) and MDA8 $[O_3]_d$ (ppbv) is the MDA8 value on $d$ day, respectively. The reason why RH is selected as the key environmental factor is that multi-linear regressions show that RH plays much more dominant roles than temperature and radiation in accounting for $O_3$ damages (see section 3.1). The thresholds of MDA8 $[O_3] = 20$ ppbv and $RH_d = 40\%$ are selected because grid-by-grid analyses show that $O_3$-induced GPP damages are very limited below those thresholds (see section 3.3).

### 2.4. $O_3$ observations

We use hourly surface $O_3$ data from the monitoring network in China, the U.S., and Europe (figure S1 (available online at stacks.iop.org/ERL/16/044030/mmedia)). These regions cover a dominant fraction of land areas suffering severe $O_3$ pollution and the consequent vegetation damages (Lu *et al* 2018, Unger *et al* 2020). The site-level $[O_3]$ over 2015–2018 are interpolated into 1° × 1° grids with missing values for grids without observational sites. The hourly $O_3$ data since 1980 in the U.S. and since 1990 in the Europe are further used to examine the trends of different metrics.

### 2.5. Multi-linear regression method

To evaluate the key environmental factors that influence $O_3$ vegetation damages, we derive the multi-linear regressions between the daily $O_3$-induced GPP damages ($GPP_d$, calculated by YIBs model) and the most related factors, including MDA8 $[O_3]$ from observations, and daily-mean temperature ($T$), RH and direct solar radiation (PAR) from MERRA2 reanalyzed data at each 1° × 1° grid:

$$\mathrm{GPP}_d = b_0 + b_1 \times \mathrm{MDA8}\,[O_3] + b_2 \times T + b_3 \times \mathrm{RH} + b_4 \times \mathrm{PAR}. \tag{9}$$

For each coefficient b ($b_1$, $b_2$, $b_3$ *and* $b_4$), the statistical significances ($P$ values) are examined by $t$-test. Finally, the factor with the minimum $P$ value is determined as the key factor at each grid.

## 3. Results

### 3.1. Key factors determine $O_3$ vegetation damage

Following the multi-linear regression method, figure 1 shows the key factors that dominate $O_3$-induced GPP damages in China, the U.S. and Europe over May to October in 2015–2018. In almost all

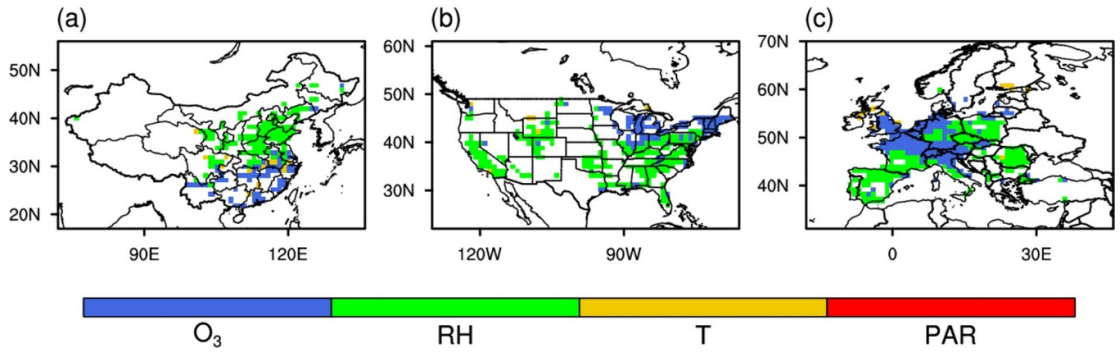


**Figure 1.** Key factors driving the $O_3$ vegetation damages in (a) China, (b) the U.S. and (c) Europe over May to October in 2015–2018 by multi-linear regressions. The daily samples of GPP damages (%), MDA8 [$O_3$] and meteorological parameters (RH, *T* and PAR) are from YIBs model simulations, ground-level observations and MERRA2 reanalyzed data, respectively. The factor at each grid with the minimum *P* value is taken as the key factor.

$1° \times 1°$ grids, $O_3$ vegetation damages are dominated by the ambient [$O_3$] or RH. Specifically, RH is more important in regions with dry climate (such as northern China, western U.S. and the Mediterranean littoral), while the MDA8 [$O_3$] drives GPP damages more in wet regions (such as southern China, eastern U.S. and the Atlantic coast in Europe). It should be noted that *T* and PAR are able to influence $g_s$ and $O_3$ stomatal uptake via determining photosynthesis rates in the Ball–Berry model, but these two factors are not dominating $O_3$-induced GPP damages based on the multi-linear regressions. As a result, we focus only on the two key factors (MDA8 [$O_3$] and RH) in the following analysis.

### 3.2. A review of $O_3$ vegetation damage with water stress

We explore the impacts of drought on $O_3$ vegetation damage from literature (table S1), which includes experiments for specific PFTs under four different conditions: (a) well-watered (WW) condition with low $O_3$ exposure (generally charcoal-filtered air); (b) WW condition with high $O_3$ exposure (generally ambient air or mixture of ambient air with $O_3$ from an $O_3$ generator); (c) reduced-water (RW) condition with low $O_3$ exposure, and (d) RW condition with high $O_3$ exposure. Generally, almost all observational studies showed that $O_3$ was more detrimental to vegetation under WW condition than RW condition. The alleviated $O_3$ damage is related to RW-induced closure of stomata that limits $O_3$ uptake. These experiments further reveal the alleviation effect of drought on $O_3$ vegetation damages, which is missing in the traditional $O_3$ exposure indexes (such as AOT40).

### 3.3. Relationships among GPP damages, MDA8 [$O_3$], and RH

The four year simulations show large GPP reductions are predicted in southeastern China, eastern U.S., and central Europe (figures 2(a)–(c)). However, these hotspots of GPP damages do not overlap with the maximum MDA8 [$O_3$] centers, which are located in north China, western U.S., and southern Europe, respectively (figures 2(d)–(f)). The dry climate facilitates $O_3$ production but leads closure of plants stomata, further inhibiting $O_3$ uptake and bringing quite low GPP damages. The spatial inconsistency between [$O_3$] and GPP damages makes the low and even negative spatial correlation coefficients of $-0.12 \sim 0.21$ between GPP reductions and [$O_3$]. Similarly, the correlations between GPP reductions and AOT40 are as low as $-0.22$–$0.24$ at these regions (figures 2(g)–(i)), suggesting that AOT40 fails in depicting reasonable spatial pattern of $O_3$ vegetation damages.

Fumigation experiments in section 3.2 show that moist conditions enhance $O_3$ vegetation damages. However, the relationships among [$O_3$], humidity, and the resultant vegetation damages are rather complex. Here, we use RH as an indicator of drought conditions and analyze the relationships among GPP reductions, MDA8 [$O_3$], and RH over all the grids throughout the four year simulations (figure 3). Large GPP reductions occur at the conditions with high MDA8 [$O_3$] and RH, though the frequency of such days/grids is limited considering increased RH is correspondent to reduced [$O_3$] (figure 3). Previous studies also revealed that high air humidity could dampen net $O_3$ production rates and consequently reduce ambient [$O_3$] (Wang *et al* 2017, Gong and Liao 2019). As a result, to depict $O_3$-induced GPP reductions, the connections between [$O_3$] and RH should be considered. Furthermore, GPP damages are moderate if MDA8 [$O_3$] is lower than 20 ppbv (figure 3) or RH is lower than 40%. For the conditions of $40\% < RH < 80\%$, GPP damages become more severe with increased RH, indicating that the stomatal opening plays an important role. However, the effects of [$O_3$] reduction by increasing RH overwhelm stomata opening if RH >80%, leading to low [$O_3$] and the consequent low GPP damages at very wet conditions.

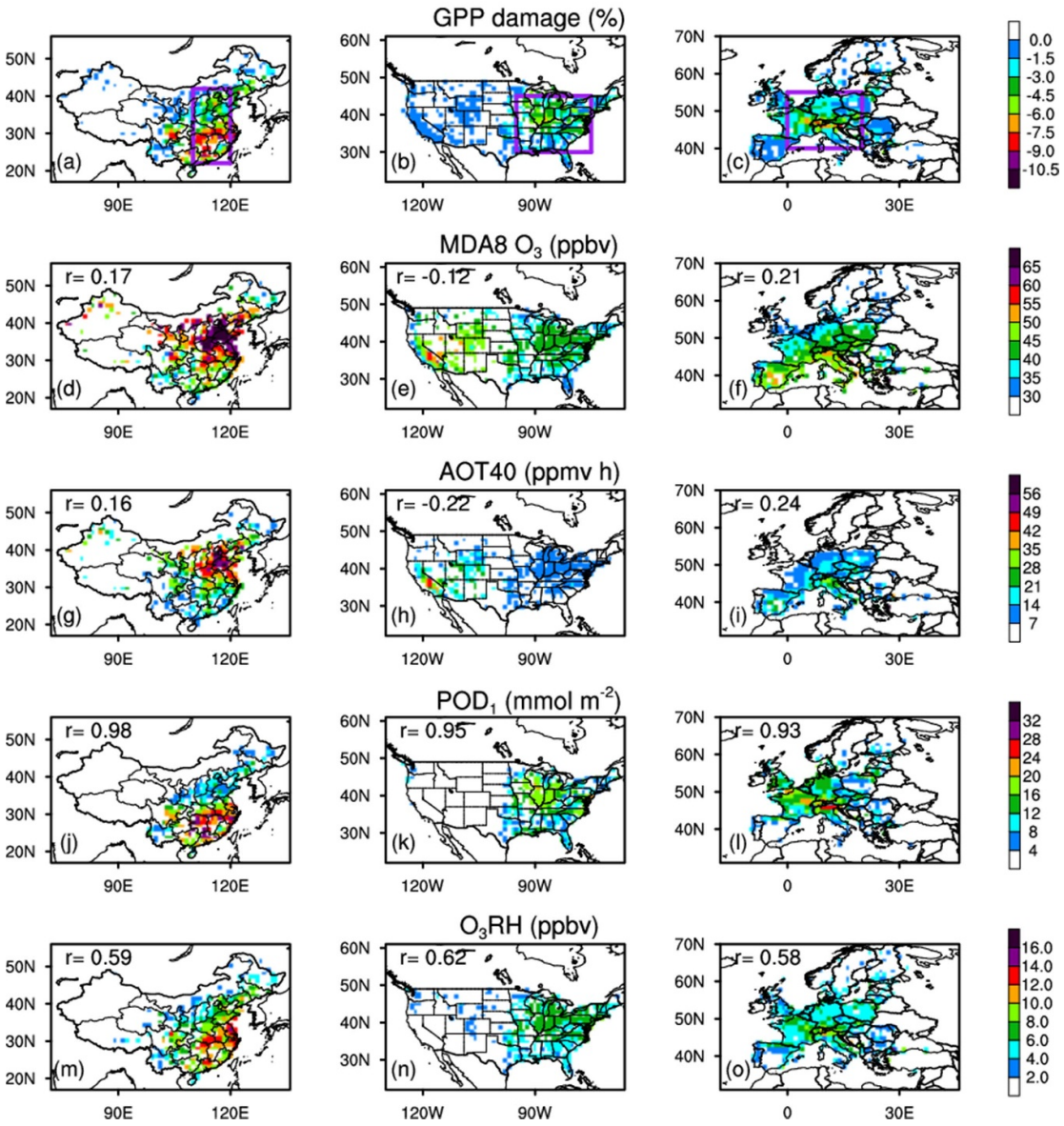


**Figure 2.** Simulated $O_3$ vegetation damages in China (left), U.S. (middle), and Europe (right) and their connections with surface MDA8 $O_3$ concentrations (second row), AOT40 (third row), $POD_1$ (fourth row), and $O_3RH$ (bottom row) over May to October in 2015–2018. The $O_3$ concentrations at 1° × 1° are interpolated from observations, based on which AOT40 and $O_3RH$ are calculated. $O_3$-induced GPP reductions and $POD_1$ are simulated by the YIBs model. The spatial correlation coefficients between different indexes and GPP reductions are shown for each region. Purple rectangles in the first row indicate regions with significant $O_3$-induced vegetation damages, including eastern China (22°–42° N, 110°–120° E), eastern U.S. (30°–45° N, 75°–95° W) and western Europe (40°–55° N, 0°–20° E).

### 3.4. Development and evaluation of $O_3RH$ index

Based on the above analyses, we propose the humidity-based index $O_3RH$ calculated with a dose-based perspective using the instantaneous MDA8 [$O_3$] and RH (section 2.3). The $O_3$ damage effects on vegetation are considered trivial if [$O_3$] is lower than 20 ppbv or RH is lower than 40%. Above those thresholds, $O_3$-induced GPP reductions are dependent on both daytime [$O_3$] and $g_s$ (equation (3)), the latter of which is positively correlated with RH (equation (1)). For the wet conditions with RH >80%, GPP damages are mainly influenced by [$O_3$], which decreases with increasing RH (figure 3).

Figures 2(j)–(o) shows the spatial patterns of $O_3RH$ averaged over May to October in 2015–2018. The correlation coefficients between GPP damages and $O_3RH$ range from 0.58 to 0.62 over China, the U.S and Europe, suggesting that the new index $O_3RH$ significantly enhances the spatial representation of GPP damages compared to the traditional dose-based AOT40 (correlation coefficients ranging from −0.22 to 0.24). In general, $O_3RH$ reflects the hotspots of $O_3$-induced damages located in wet regions with relatively high $O_3$ concentrations, such as southeastern China, eastern U.S., and central Europe. However, the $O_3RH$ index ignores varied $O_3$ sensitivities among

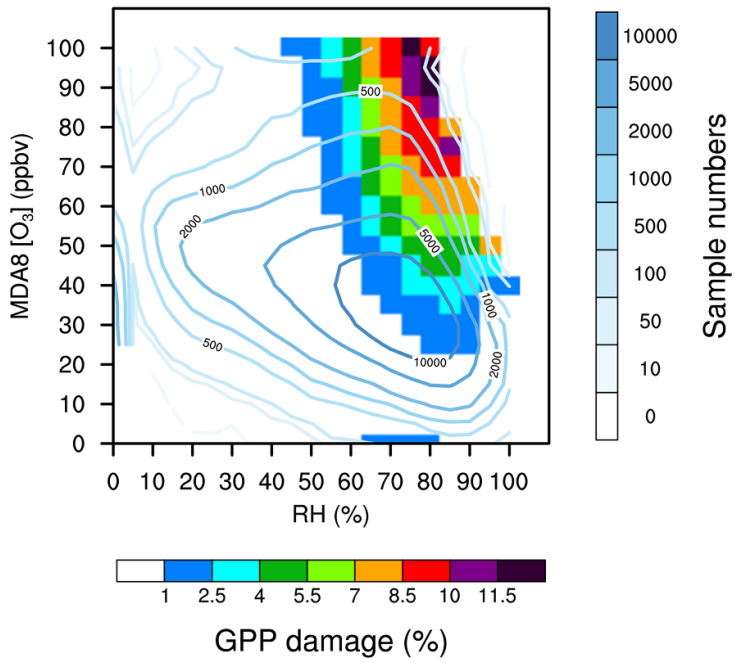


**Figure 3.** Relationships among the ambient $O_3$ concentrations, RH, and the percentage of GPP damages. All the daily samples from the 1° × 1° grids in figure 2 are collected and aggregated into different bins of $O_3$ concentrations and RH. For each bin, the average GPP damages is shown as filled patches and the number of samples is shown as colored contours.

different plant species, leading to lower spatial consistency between $O_3$RH and GPP damages than that between $POD_1$ and GPP damages (figures 2(j)–(l)).

Figure S2 examines the temporal correlations between simulated GPP damages and different metrics over three selected regions (shown in figures 2(a)–(c)). The exposure-based metrics like MDA8 [$O_3$] and AOT40 perform best in western Europe (40°–55° N, 0°–20° E) with correlation coefficients of 0.8 and 0.79. However, these indexes show medium correlations (0.65 and 0.67) over eastern U.S. (30°–45° N, 75°–95° W), and poor correlations (0.41 and 0.50) in eastern China (22°–42° N, 110°–120° E). It reveals that the traditional exposure-based index AOT40, which is originally proposed to evaluate the $O_3$ ecological effects over Europe (Fuhrer *et al* 1997), should be used with cautions over regions outside Europe due to the missing of regulations by water stress. As a comparison, the new $O_3$RH index shows regionally consistent high temporal correlation coefficients (0.73–0.82) with local GPP damages, highlighting the importance of water stress in regulating $O_3$-induced vegetation damages.

### 3.5. Application of the $O_3$RH index

With the $O_3$RH index, we expect to estimate $O_3$-induced GPP damages as reasonable as DGVM simulations. Figure S3 compares the $O_3$RH with GPP percentage damages ($GPP_d$ (%)) over May to October simulated by YIBs model over China, the U.S and Europe. Over these regions, high $R^2$ from 0.60 to 0.75 are predicted between $O_3$RH and $GPP_d$ (table S2). Such correlations are much higher than the $R^2$ of 0.24–0.47 between AOT40 and $GPP_d$, indicating the improvement of $O_3$RH in describing the $O_3$ ecological effects. We further calculate the linear regression between $O_3$RH and $GPP_d$ (%) as follows:

$$GPP_d\,(\%) = 0.65 \times O_3RH - 0.92. \qquad (10)$$

The average slope of 0.65 is accompanied by a range of uncertainties from 0.51 to 0.77 for different years at different regions (table S2).

We further examine the long-term trends of $O_3$-induced GPP damages with different metrics based on site-level observations (figure 4). Surface MDA8 [$O_3$] significantly reduces by 0.142 ppbv $yr^{-1}$ in eastern U.S. from 1980 to 2018 and 0.086 ppbv $yr^{-1}$ in western Europe from 1990 to 2017 (figure 4(a)). Meanwhile, MDA8 [$O_3$] shows significant enhancement of 2.58 ppbv $yr^{-1}$ in China during 2014–2018. The trends of AOT40 show consistent and significant changes as that of MDA8 [$O_3$], with reductions in eastern U.S. and western Europe but enhancement in China (figure 4(b)). However, trends of $O_3$RH are moderate and insignificant for both eastern U.S. and western Europe (figure 4(c)), in part attributed to the positive trends in RH (not shown). As a result, estimates based on $O_3$RH suggest that declining [$O_3$] failed to bring expected lower $O_3$ vegetation damages in these two regions. Such conclusion is consistent with regional studies using observations (Ronan *et al* 2020) and DGVMs (Yue *et al* 2016).

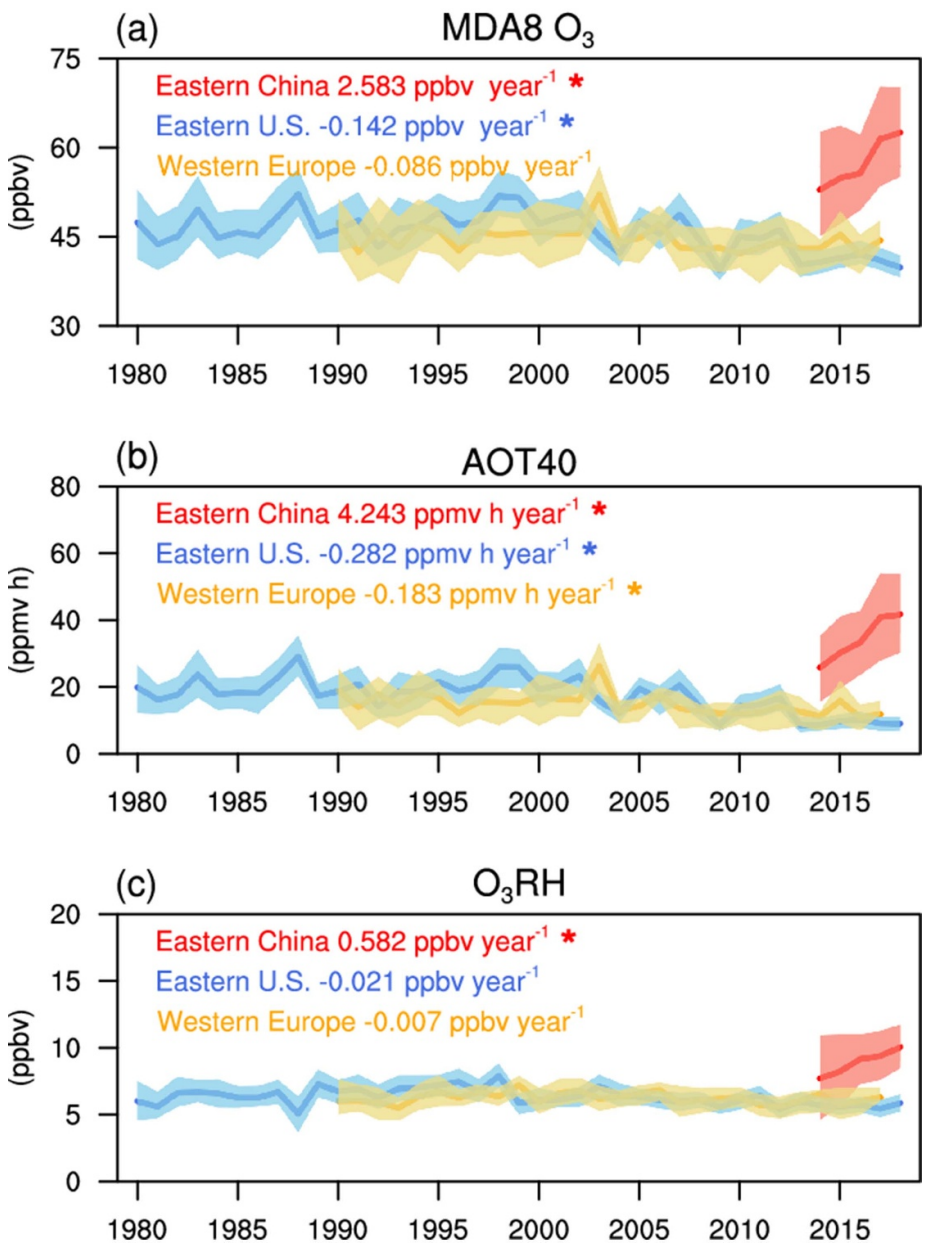


**Figure 4.** The temporal variations of May–October (a) MDA8 [$O_3$], (b) AOT40 and (c) $O_3$RH averaged over eastern China (2014–2018, red lines), eastern U.S. (1980–2018, blue lines) and western Europe (1990–2017, gold lines). The locations of observational sites are shown in figure S1. Colored shades indicate the ranges between the first and third quartiles of the site samples in each region. Trends significant at the $P < 0.01$ level are indicated by the asterisks.

## 4. Discussions

In this study, we proposed a new humidity-based index $O_3$RH to simplify the calculation of $O_3$ vegetation damage but with comparable accuracy to dose-based indexes or simulations by DGVMs. The $O_3$RH index provides a bridge between atmospheric chemistry community and ecological science community by considering the key environmental factors that influencing $O_3$ vegetation damages. With the help of $O_3$RH, it becomes possible to assess reasonable regional or global $O_3$-induced vegetation damages only by normal ground-level $O_3$ and meteorological observations without expensive and complex experiments. For policy makers, $O_3$RH is a more scientific and reliable index to evaluate $O_3$ ecological effects relative to the traditional exposure indexes.

However, the $O_3$RH is also confronted with various sources of uncertainties. First, the index adopts MDA8 [$O_3$] and daily RH, thus ignoring the impacts of diurnal variations on $O_3$ vegetation damages. Also, some studies assessed $O_3$ vegetation damages by accumulated $O_3$ metrics (e.g. Bueker *et al* 2015, Lombardozzi *et al* 2015), leading higher vegetation damages at the end of growth season. Such effects cannot be represented by the instantaneous daily $O_3$RH index. Second, air humidity instead of soil moisture is applied in the parameterization, because

observations of soil moisture are much more difficult than RH. Many studies have showed the important roles of soil water content in regulating stomatal activities (Hayes *et al* 2012, De Marco *et al* 2016, CLRTAP 2017). Although the soil moisture and air RH show high temporal correlations (figure S4), it remains unclear how the differences between RH and soil water stress may influence the accuracy of index. Third, the varied sensitivities of different PFTs to $O_3$ are not considered in $O_3$RH. Observations show that plants have different sensitivities to the same dose of stomatal $O_3$ fluxes (Sitch *et al* 2007, Bueker *et al* 2015). Omissions of PFT-specific characteristics may result in biases of predicted vegetation damages.

The calibration and validation of $O_3$RH are dependent on the a process-based DGVM (YIBs) and a semi-mechanistic $O_3$ vegetation damages Sitch *et al* (2007) scheme in this study. The model dependence may also bring uncertainties. For example, the $1° \times 1°$ resolution remains too coarse to reflect the high spatial variability of $[O_3]$ and meteorological factors. Furthermore, Sitch *et al* (2007) scheme derives GPP damages by the instantaneous $F_{O3}$. However, some studies also reported the sluggish effects that stomata lost functions under $O_3$ exposure (Paoletti and Grulke 2010, Hoshika *et al* 2014, Lombardozzi *et al* 2015), which is difficult to be represented in Sitch *et al* (2007) scheme. The extraordinary high correlations between GPP damages and $POD_1$ (figures 2(j)–(l)) are also attributed to the $F_{O3}$ dependent scheme even though most filed experiments show correlations coefficients between vegetation damages and $POD_Y$ generally lower than 0.8 (Bueker *et al* 2015, Convention *et al* 2017).

Despite these uncertainties, we demonstrate that the $O_3$RH index is a simplified but effective way to assess regional $O_3$ vegetation damages. We suggest the substitution of traditional AOT40 with $O_3$RH to account for the regulation by water stress. Analyses using $O_3$RH show that $O_3$ vegetation damages continue increasing in China and remain stable in eastern U.S. and western Europe during the past several years and decades. Such trends pose a long-lasting threat by surface $O_3$ to global ecosystems.

## 5. Conclusion

To overcome the poor spatiotemporal representations of traditional $O_3$ exposure indexes and disadvantages of dose-based indexes in complex and skilled calculations, a new humidity-based index $O_3$RH was proposed in this study to better assess the $O_3$ ecological effects. We firstly selected RH and $[O_3]$ as the key factors determining the magnitudes of $O_3$-indced vegetation damages by multi-linear regressions, and then explored the relationships among $[O_3]$, RH and GPP damages with the help of YIBs model. The simulation as well as field experiments from literature both supported that moist conditions enhance $O_3$ vegetation damages. Based on these analyses, $O_3$RH was proposed and evaluated, which showed better spatiotemporal variation of $O_3$-induced GPP reductions than the AOT40 index. Applications of $O_3$RH index show that the decline of $[O_3]$ over the past several decades cannot relieve $O_3$ vegetation damages in eastern U.S and western Europe. Meanwhile, the fast increases of surface $[O_3]$ boost damages to vegetation in China. Our results showed that $O_3$RH was able to be calculated as easy as exposure-based indexes (not dependent on any expensive observations or numerical models) and had similar spatiotemporal representation of $O_3$ damage as dose-based method, which greatly facilitated the assessment of $O_3$ vegetation damages, especially for policy makers and researchers without ecological backgrounds.

## Data availability statement

The data that support the findings of this study are available upon reasonable request from the authors.

## Acknowledgments

This work was jointly supported by the National Key Research and Development Program of China (Grant No. 2019YFA0606802), the National Natural Science Foundation of China (Grant Nos. 41975155, 42021004, and 91744311), and the Jiangsu Science Fund for Distinguished Young Scholars (Grant No. BK20200040). The authors acknowledge the Data Center of China's Ministry of Ecology and Environment, the US Environmental Protection Agency, the EMEP and European Environment Agency for providing ozone data publicly.

## Conflict of interest

The authors declare no competing financial interest.

## ORCID iDs

Cheng Gong https://orcid.org/0000-0002-3434-6232
Xu Yue https://orcid.org/0000-0002-8861-8192

## References

Anav A, De Marco A, Proietti C, Alessandri A, Dell'Aquila A, Cionni I, Friedlingstein P, Khvorostyanov D, Menut L and Paoletti E 2016 Comparing concentration-based (AOT40) and stomatal uptake (PODY) metrics for ozone risk assessment to European forests *Glob. Change Biol.* **22** 1608–27

Anav A, DeMarco A, Friedlingstein P, Savi F, Sicard P, Sitch S, Vitale M and Paoletti E 2019 Growing season extension affects ozone uptake by European forests *Sci. Total Environ.* **669** 1043–52

Arnold S R, Lombardozzi D, Lamarque J F, Richardson T, Emmons L K, Tilmes S, Sitch S A, Folberth G, Hollaway M J

and Martin M V 2018 Simulated global climate response to tropospheric ozone-induced changes in plant transpiration *Geophys. Res. Lett.* **45** 13070–9

Atkinson R 2000 Atmospheric chemistry of VOCs and $NO_x$ *Atmos. Environ.* **34** 2063–101

Ball J T, Woodrow I E and Berry J A 1987 A model predicting stomatal conductance and its contribution to the control of photosynthesis under different environmental conditions *Prog. Photosynth. Res.* **4** 221–4

Buckley T N and Mott K A 2013 Modelling stomatal conductance in response to environmental factors *Plant Cell Environ.* **36** 1691–9

Bueker P *et al* 2012 DO3SE modelling of soil moisture to determine ozone flux to forest trees *Atmos. Chem. Phys.* **12** 5537–62

Bueker P *et al* 2015 New flux based dose-response relationships for ozone for European forest tree species *Environ. Pollut.* **206** 163–74

Clifton O E *et al* 2020a Dry deposition of ozone over land: processes, measurement, and modeling *Rev. Geophys.* **58** e2019RG000670

Clifton O E, Lombardozzi D L, Fiore A M, Paulot F and Horowitz L W 2020b Stomatal conductance influences interannual variability and long-term changes in regional cumulative plant uptake of ozone *Environ. Res. Lett.* **15** 114059

CLRTAP 2017 Chapter III of Manual on methodologies and criteria for modelling and mapping critical loads and levels and air pollution effects, risks and trends *Mapping Critical Levels for Vegetation* (http://icpvegetation.ceh.ac.uk/)

De Marco A, Anav A, Sicard P, Feng Z and Paoletti E 2020 High spatial resolution ozone risk-assessment for Asian forests *Environ. Res. Lett.* **15** 104095

De Marco A, Sicard P, Fares S, Tuovinen J-P, Anav A and Paoletti E 2016 Assessing the role of soil water limitation in determining the phytotoxic ozone dose (PODY) thresholds *Atmos. Environ.* **147** 88–97

Emberson L D, Ashmore M R, Cambridge H M, Simpson D and Tuovinen J P 2000 Modelling stomatal ozone flux across Europe *Environ. Pollut.* **109** 403–13

Farquhar G D, Von Caemmerer S V and Berry J A 1980 A biochemical model of photosynthetic $CO_2$ assimilation in leaves of $C_3$ species *Planta* **149** 78–90

Feng Z, De Marco A, Anav A, Gualtieri M, Sicard P, Tian H, Fornasier F, Tao F, Guo A and Paoletti E 2019 Economic losses due to ozone impacts on human health, forest productivity and crop yield across China *Environ. Int.* **131** 104966

Fuhrer J, Skarby L and Ashmore M R 1997 Critical levels for ozone effects on vegetation in Europe *Environ. Pollut.* **97** 91–106

Gao F, Catalayud V, Paoletti E, Hoshika Y and Feng Z 2017 Water stress mitigates the negative effects of ozone on photosynthesis and biomass in poplar plants *Environ. Pollut.* **230** 268–79

Gong C, Lei Y, Ma Y, Yue X and Liao H 2020 Ozone-vegetation feedback through dry deposition and isoprene emissions in a global chemistry-carbon-climate model *Atmos. Chem. Phys.* **20** 3841–57

Gong C and Liao H 2019 A typical weather pattern for ozone pollution events in North China *Atmos. Chem. Phys.* **19** 13725–40

Hayes F, Wagg S, Mills G, Wilkinson S and Davies W 2012 Ozone effects in a drier climate: implications for stomatal fluxes of reduced stomatal sensitivity to soil drying in a typical grassland species *Glob. Change Biol.* **18** 948–59

Hoshika Y, Carriero G, Feng Z, Zhang Y and Paoletti E 2014 Determinants of stomatal sluggishness in ozone-exposed deciduous tree species *Sci. Total. Environ.* **481** 453–8

Jacob D J and Winner D A 2009 Effect of climate change on air quality *Atmos. Environ.* **43** 51–63

Jarvis P G 1976 Interpretation of variations in leaf water potential and stomatal conductance found in canopies in field *Phil. Trans. R. Soc.* B **273** 593–610

Karlsson P E *et al* 2004 New critical levels for ozone effects on young trees based on AOT40 and simulated cumulative leaf uptake of ozone *Atmos. Environ.* **38** 2283–94

Karlsson P E *et al* 2007 Risk assessments for forest trees: the performance of the ozone flux versus the AOT concepts *Environ. Pollut.* **146** 608–16

Khan S and Soja G 2003 Yield responses of wheat to ozone exposure as modified by drought-induced differences in ozone uptake *Water Air. Soil Pollut.* **147** 299–315

Kleinman L I 2005 The dependence of tropospheric ozone production rate on ozone precursors *Atmos. Environ.* **39** 575–86

Lin Y, Jiang F, Zhao J, Zhu G, He X, Ma X, Li S, Sabel C E and Wang H 2018 Impacts of O-3 on premature mortality and crop yield loss across China *Atmos. Environ.* **194** 41–47

Lombardozzi D, Levis S, Bonan G, Hess P G and Sparks J P 2015 The influence of chronic ozone exposure on global carbon and water cycles *J. Clim.* **28** 292–305

Lombardozzi D, Levis S, Bonan G and Sparks J P 2012 Predicting photosynthesis and transpiration responses to ozone: decoupling modeled photosynthesis and stomatal conductance *Biogeosciences* **9** 3113–30

Lu X, Hong J, Zhang L, Cooper O R, Schultz M G, Xu X, Wang T, Gao M, Zhao Y and Zhang Y 2018 Severe surface ozone pollution in china: a global perspective *Environ. Sci. Technol. Lett.* **5** 487–94

Mills G *et al* 2011b New stomatal flux-based critical levels for ozone effects on vegetation *Atmos. Environ.* **45** 5064–8

Mills G *et al* 2018 Tropospheric ozone assessment report: present-day tropospheric ozone distribution and trends relevant to vegetation *Elementa Sci. Anthrop.* **6** 47

Mills G, Hayes F, Simpson D, Emberson L, Norris D, Harmens H and Bueker P 2011a Evidence of widespread effects of ozone on crops and (semi-)natural vegetation in Europe (1990–2006) in relation to AOT40-and flux-based risk maps *Glob. Change Biol.* **17** 592–613

Mishra A K, Rai R and Agrawal S B 2013 Differential response of dwarf and tall tropical wheat cultivars to elevated ozone with and without carbon dioxide enrichment: growth, yield and grain quality *Field Crop Res.* **145** 21–32

Molod A, Takacs L, Suarez M and Bacmeister J 2015 Development of the GEOS-5 atmospheric general circulation model: evolution from MERRA to MERRA2 *Geosci. Model Dev.* **8** 1339–56

Musselman R C, Lefohn A S, Massman W J and Heath R L 2006 A critical review and analysis of the use of exposure- and flux-based ozone indices for predicting vegetation effects *Atmos. Environ.* **40** 1869–88

Paakkonen E, Vahala J, Pohjolai M, Holopainen T and Karenlampi L 1998 Physiological, stomatal and ultrastructural ozone responses in birch (Betula pendula Roth.) are modified by water stress *Plant Cell Environ.* **21** 671–84

Paoletti E and Grulke N E 2010 Ozone exposure and stomatal sluggishness in different plant physiognomic classes *Environ. Pollut.* **158** 2664–71

Ronan A C, Ducker J A, Schnell J L and Holmes C D 2020 Have improvements in ozone air quality reduced ozone uptake into plants? *Elementa Sci. Anthrop.* **8** 2

Sadiq M, Tai A P K, Lombardozzi D and Martin M V 2017 Effects of ozone-vegetation coupling on surface ozone air quality via biogeochemical and meteorological feedbacks *Atmos. Chem. Phys.* **17** 3055–66

Shang B, Feng Z, Li P, Yuan X, Xu Y and Calatayud V 2017 Ozone exposure-and flux-based response relationships with photosynthesis, leaf morphology and biomass in two poplar clones *Sci. Total Environ.* **603** 185–95

Sicard P 2020 Ground-level ozone over time: an observation-based global overview *Curr. Opin. Environ. Sci. Health* **19** 100226

Sicard P, Anav A, De Marco A and Paoletti E 2017 Projected global ground-level ozone impacts on vegetation under different

emission and climate scenarios *Atmos. Chem. Phys.* **17** 12177–96

Sicard P, Serra R and Rossello P 2016 Spatiotemporal trends in ground-level ozone concentrations and metrics in France over the time period 1999–2012 *Environ. Res.* **149** 122–44

Sitch S, Cox P M, Collins W J and Huntingford C 2007 Indirect radiative forcing of climate change through ozone effects on the land-carbon sink *Nature* **448** 791-U4

Spranger T, Lorenz U and Gregor H 2004 Manual on methodologies and criteria for modelling and mapping critical loads & levels and air pollution effects, risks and trends (https://www.umweltbundesamt.de/en/publikationen/manual-on-methodologies-criteria-for-modelling)

Thomas V F D, Braun S and Fluckiger W 2006 Effects of simultaneous ozone exposure and nitrogen loads on carbohydrate concentrations, biomass, growth, and nutrient concentrations of young beech trees (Fagus sylvatica) *Environ. Pollut.* **143** 341–54

Tian H *et al* 2011 China's terrestrial carbon balance: contributions from multiple global change factors *Glob. Biogeochem. Cycles* **25** 1

Topa M A, McDermitt D J, Yun S C and King P S 2004 Do elevated ozone and variable light alter carbon transport to roots in sugar maple? *New Phytol.* **162** 173–86

Unger N, Zheng Y, Yue X and Harper K L 2020 Mitigation of ozone damage to the world's land ecosystems by source sector *Nat. Clim. Change* **10** 134

Vingarzan R 2004 A review of surface ozone background levels and trends *Atmos. Environ.* **38** 3431–42

Wang T, Xue L, Brimblecombe P, Lam Y F, Li L and Zhang L 2017 Ozone pollution in China: a review of concentrations, meteorological influences, chemical precursors, and effects *Sci. Total Environ.* **575** 1582–96

Yue X, Keenan T F, Munger W and Unger N 2016 Limited effect of ozone reductions on the 20 year photosynthesis trend at Harvard forest *Glob. Change Biol.* **22** 3750–9

Yue X and Unger N 2015 The yale interactive terrestrial biosphere model version 1.0: description, evaluation and implementation into NASA GISS ModelE2 *Geosci. Model Dev.* **8** 2399–417

Yue X and Unger N 2018 Fire air pollution reduces global terrestrial productivity *Nat. Commun.* **9** 1–9

Yue X, Unger N, Harper K, Xia X, Liao H, Zhu T, Xiao J, Feng Z and Li J 2017 Ozone and haze pollution weakens net primary productivity in China *Atmos. Chem. Phys.* **17** 6073–89